https://doi.org/10.1016/j.buildenv.2018.04.037

Wind weakening in a dense high-rise city due to over nearly five decades of urbanization

Lei Peng[1], Jia-Ping Liu[2], Yi Wang[3], Pak-wai Chan[4], Tsz-cheung Lee[4], Fen Peng[5], Man-sing Wong[6], Yuguo Li[1]*

[1]Department of Mechanical Engineering, The University of Hong Kong, Pokfulam, Hong Kong, China
[2]College of Architecture, Xi'an University of Architecture and Technology, Xi'an, China
[3]School of Environmental and Municipal Engineering, Xi'an University of Architecture and Technology, Xi'an, China
[4]Hong Kong Observatory, Hong Kong, China
[5]Changsha University of Science and Technology, Changsha, China
[6]Department of Land Surveying and Geo-Informatics, The Hong Kong Polytechnic University, Hong Kong, China

***Correspondence author:** Yuguo Li, liyg@hku.hk

HIGHLIGHTS

- Investigated evolution of historical wind environment in a dense high-rise city.
- Provided evidence that continuous urbanization can lead to significant wind speed reduction within a densely developed city.
- In the case study of the Kowloon Peninsula in Hong Kong, total wind loss rates within an elevation of 200 m increased from less than 10% to larger than 20% from 1964 to 2010 andfuture total wind loss rate may increase to about 40% by 2050 if the current weakening trend continues.

ABSTRACT

Decreasing trends of near-surface wind speed in urban areas, particularly in high-rise compact settings, have been identified in the past few decades. At the King's Park meteorological station in the heart of the Kowloon Peninsula Hong Kong, a wind speed reduction of 0.6 m/s per decade was observed from 1968 to 1995, and 0.12 m/s per decade since 1995. We obtained data on the changing three-dimensional urban morphology of Kowloon during the period of 1964-2010, and conducted computational fluid dynamics simulations on historical wind environment considering the prevailing winds. The wind speed and its loss were calculated as both intrinsic and comprehensive spatial averages within an elevation of 200 m. The results show that the overall mean wind speed in the studied urban areas gradually decreased due to the continuous urban development and elevation in building height. The total wind loss rates at three representative locations have increased from less than 10% to greater than 20% during the study period. The total wind loss rate may increase to about 40% by 2050 if the current weakening trend continues. Although the average wind speed at pedestrian level has significantly declined, local acceleration of wind was observed in some local areas. However, such accelerated airflow is only maintained around a few blocks of buildings. Our study demonstrates the impact of urbanization on the wind weakening in Hong Kong and reveals the importance and need of factoring in urban air ventilation into the design of urban morphology.

KEYWORDS: wind loss, wind weakening, CFD, urban environment, Hong Kong

1. Introduction

Globally, the observed near-surface wind speed has significantly decreased over all continents [1-3]. The annual mean wind speeds declined at 73% of 822 surface stations over the 1979-2008 period [3]. In South Asia, Europe, Central Asia, Eastern Asia, and North America, the annual mean surface wind speed has decreased on average at a rate of -0.08, -0.09, -0.16, -0.12, and -0.07 m/s per decade, respectively (i.e. -5%, -2.9%, -5.9%, -4.2%, and -1.8% per decade). This represents a decrease of more than 10% in 30 years in Asia. From 1969 to 1990, the near-surface wind speed in China decreased by 0.031 m/year and 0.028 m/year at urban and rural stations, respectively [1]. However, none of the above-cited studies explored the exact causes of wind weakening.

The winds in cities are weakening at a much faster rate than in other areas. In Athens, Greece, winds can be reduced by up to 10 times in urban canyons compared with the undisturbed ambient wind [4]. The wind speed above buildings is predicted to be reduced by 40% in Lisbon if the aerodynamic roughness is increased from 0.02 m to 1.5 m [5]. The urban population worldwide has rapidly increased from only 30% in 1950 to 54% in 2014 [6]. The dense development in a crowded city may have significant impacts on the urban climate. In particular, the weakening of wind tends to hinder the removal of airborne pollutants, anthropogenic moisture, and heat, while exacerbating urban heat stress, and increasing the rate of energy consumption by buildings[9, Lam, 2006; Ng, 2009; Lee et al., 2010]. As such, with a view to mitigating these negative effects and improving the quality of living environment, sufficient wind is essential for the natural ventilation of the city.

As local wind is one of the key factors determining the urban microclimate and human thermal comfort [HKGBC, 2017], an in-depth understanding of the mechanism and extent of wind loss due to urbanization is increasingly important, especially for climate scientists, urban planners and policy makers. Building densification is likely one of the primary causes of the wind stilling in urban areas; however, the effects of building density and height on local wind weakening have not been explored in many places.

Hong Kong, situated at the southeastern coast of China and over the eastern part of the Pearl River Delta, has developed from a trading port in mid-19th century into a modern and highly urbanized metropolitan coastal city with about 7.4 million people today. While Hong Kong has a total area of about 1104 km^2, owing to its mountainous topography with steep slopes over 20 percent of the total land area, most of the urban activities are concentrated on built-up areas which take up about 24 percent of land [DEVB, 2017]. Therefore, Hong Kong is a good location for a case study of the issue of urban wind speed reduction. Wind speed in Hong Kong has declined significantly in recent decades [7; Lai et al., 2014]. The rapid development of Hong Kong has involved the continuous building or reconstruction of many new high-rise buildings. Kowloon Peninsula, a densely built-up area with only 4.24% of the land but 30.6% of the population of Hong Kong as of mid-2016 [8], has undergone particularly intense urbanization in the past 50 years. The annual mean wind speed recorded at the King's Park Meteorological Station which is located at the heart of the Kowloon Peninsula has declined by a remarkable -0.6 m/s per decade from 1968 to 1995 and -0.12 m/s per decade since then, vastly exceeding the national or continental rates of wind stilling. Here we take Kowloon as a representative case to investigate the impact of urbanization on the wind speed reduction.

Quantifying the impact of urbanization on wind speed reduction across decades is not an easy task. Several researchers have attempted to address this issue by both measurements and simulations. Liu et al. [10] found that urbanization had a profound impact on wind speed, based on observations at 15 altitudes from a 325 m meteorological tower located in an area transitioning from a suburban to an urban district. The local aerodynamic roughness length and zero-plane displacement height were found to double from 1991-2011. Although that study provided an insight into the significant change of urban roughness, the total number of observation sites was quite limited; indeed, it is not practical to conduct large-scale field measurements spanning multiple decades. Hou et al. [11] concluded that the urbanization in Beijing from the 1960s to 2000s contributed to about 35% of the wind stilling, on the basis of Weather Research and Forecasting Model (WRF) simulations. Although this meso-scale model can simulate the flow on a very large scale, it simplifies the roughness elements near the surface, and therefore cannot capture the detailed airflows within the urban canopy layer to discern the underlying physics. Hence, field-scale experiments and computational fluid dynamics (CFD) simulations are the most appropriate approaches to investigate city-scale wind environments.

Recently, many studies have been conducted on ideal and real building configurations by using scaled wind-tunnel experiments, water tank modeling, and full-scale field monitoring [12-14], and both ideal [15] and resolved urban morphologies have been well studied by numerical simulations. With improved computer power, detailed CFD simulations with well resolved urban morphology on large scales have been conducted in the past 20 years, e.g. in Hong Kong [16], London [17], Tokyo [18], and Niigata City [19]. CFD simulations have proven to be an efficient, accurate, and economical tool to study the evolution of city-scale airflows.

This study applied CFD simulations with resolved buildings in historical wind environments in Kowloon, Hong Kong from 1964 to 2010, to explore the influence of continuous urbanization. Eight historical urban morphology datasets during the period were generated based on orthophotos, digital surface models (DSMs), and digital elevation models (DEMs) with the aid of historical aerial photographs [20]. A realizable k-ε model was used following earlier studies of airflow around buildings and complex terrain [21,22]. The predicted averaged mean wind speed was compared at several representative locations in different years, and the wind loss rate was also calculated using the predicted vertical wind profiles, and analyzed.

This paper is organized as follows. Section 2 describes the data and numerical procedure, followed by the results and analysis in Section 3. Finally, Section 4 presents the conclusions.

2. Methods

2.1 Historical data of wind and buildings

Hourly mean wind speed and direction observations from four weather monitoring stations in Hong Kong, including King's Park Meteorological Station (KP, 22°18'43"N 114°10'22"E), Star Ferry station (SF, 22°17'35"N 114°10'07"E), Kai Tak station (KT, 22°18'35"N 114°12'48"E), and Waglan Island station (WGL, 22°10'56"N 114°18'12"E), were obtained from Hong Kong Observatory (HKO), the meteorological authority of Hong Kong. The locations of Hong Kong and these stations are shown in Fig. 1A and 1B respectively. WGL is

a remote island over open sea to the southeast of Hong Kong Island, and it is considered as the source of "background wind" into the city (data available since 1968). The KT station (data available since1998) can be considered as the upstream station measuring the wind approaching the Kowloon Peninsula from the east (i.e. the prevailing wind direction of Hong Kong). KP station is located in central Kowloon, as shown, in a relatively open area. SF station is located at the southern tip of the Kowloon Peninsula. The wind data at KP and SF is available since 1968 and 1987, respectively.

The building footprints were reconstructed based on orthophotos and DSMs, referring to the building footprints of 2010 from the Hong Kong Lands Department. The building heights were computed by subtracting the DSM from the LiDAR DEM retrospectively [20]. The mean absolute error (MAE) of building height is 0.81-3.25 m (Table 1).

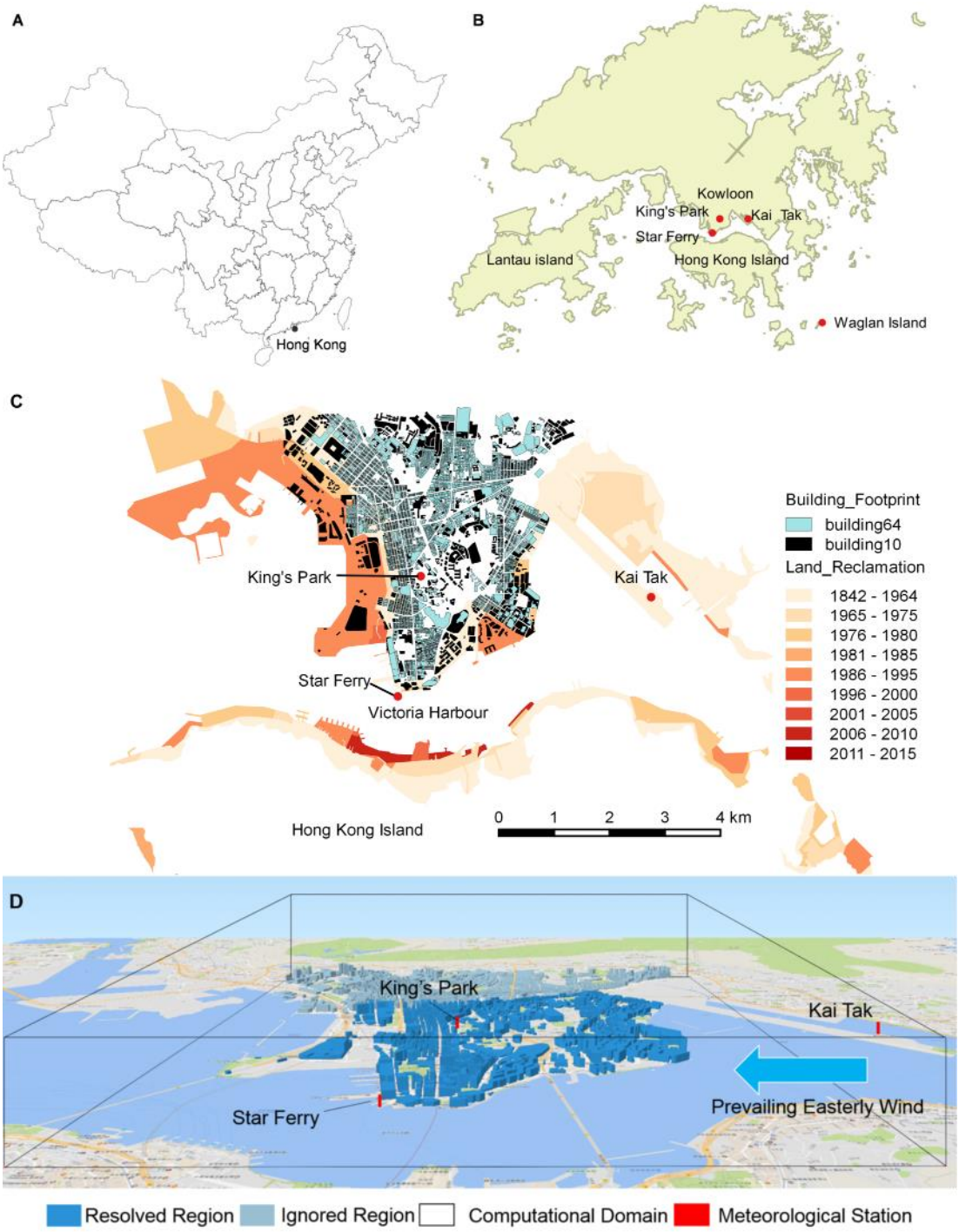

Fig. 1. (A) Location of Hong Kong; (B) location of King's Park (KP), Star Ferry (SF), Kai Tak (KT), and Waglan Island (WI) meteorological stations; (C) building footprints in 1964 and 2010 and history of land reclamation; (D) perspective view of Kowloon Peninsula in 2010 and the locations of the meteorological stations.

Fig. 1C represents the detailed building footprints of Kowloon in 1964 and 2010 in blue and black, respectively. Many land reclamation projects have been conducted along the former coastline, and many buildings have been built on the new land. We chose to study the urban areas in the southern and middle regions of Kowloon in 2010, indicated in dark blue in Fig. 1D. The two meteorological stations located at KP and SF, which provide validation information, are also shown. 3D building data are available for eight different years, as

shown in Fig. 2.

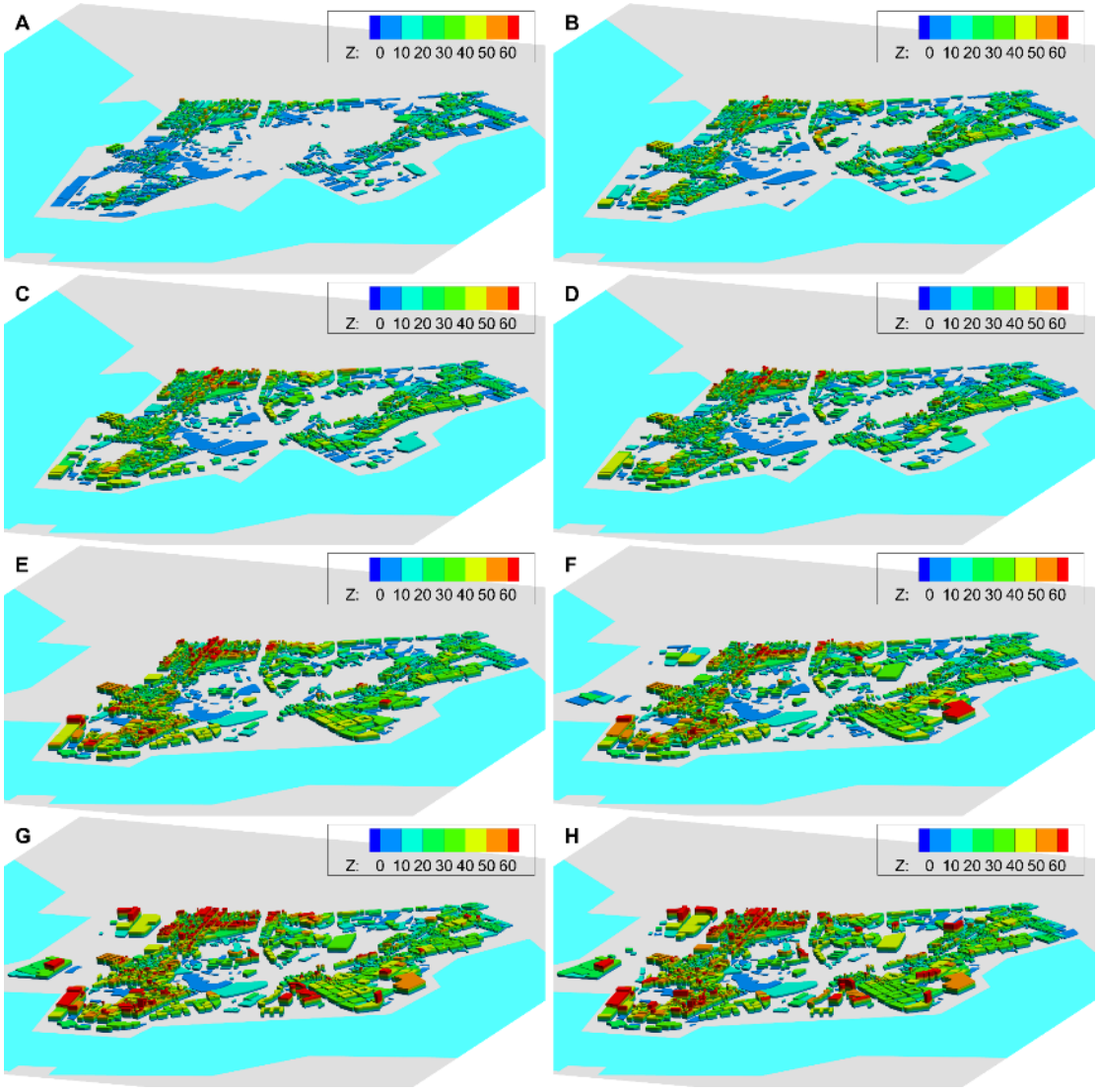

Fig. 2. Layout of buildings in eight different years from 1964 to 2010. (A: 1964, B: 1975, C: 1980, D: 1985, E: 1995, F: 2000, G: 2005, H: 2010.)

2.2 CFD modeling

Fig. 2 shows the building layouts in the investigated regions in different years. The computational domain is 6km × 6km × 1km for all cases, which covers buildings across a large area in the horizontal and vertical directions. The south and center of Kowloon were included because these areas have undergone the most significant development, and the KP and SF stations are both located in these regions. The blockage ratio in the computational domain is less than 3%. Extensions of 5H are created in the upstream and lateral directions, and of 10H in the downstream direction, following the Architectural Institute of Japan (AIJ)'s guidelines [23].

The simulations were conducted using the commercial CFD software Fluent. The 3D steady RANS equations were solved under isothermal conditions. A total of eight cases were simulated, with each case corresponding to a year for which the 3D building data are available. Hybrid meshes consisting of hexahedral and prismatic cells were generated by

sweep and extrusion of a 2D surface mesh, with reference to the mesh generation technique presented by van Hooff and Blocken [24]. The procedure was conducted with the aid of the pre-processing software ICEM CFD, resulting in 12.6 to 14.9 million cells (Table 1) based on a grid-sensitivity analysis of mean wind speed in the built area. Fig. 3B and 3C show a part of the mesh of Case H and a perspective view extracted from Google Earth.

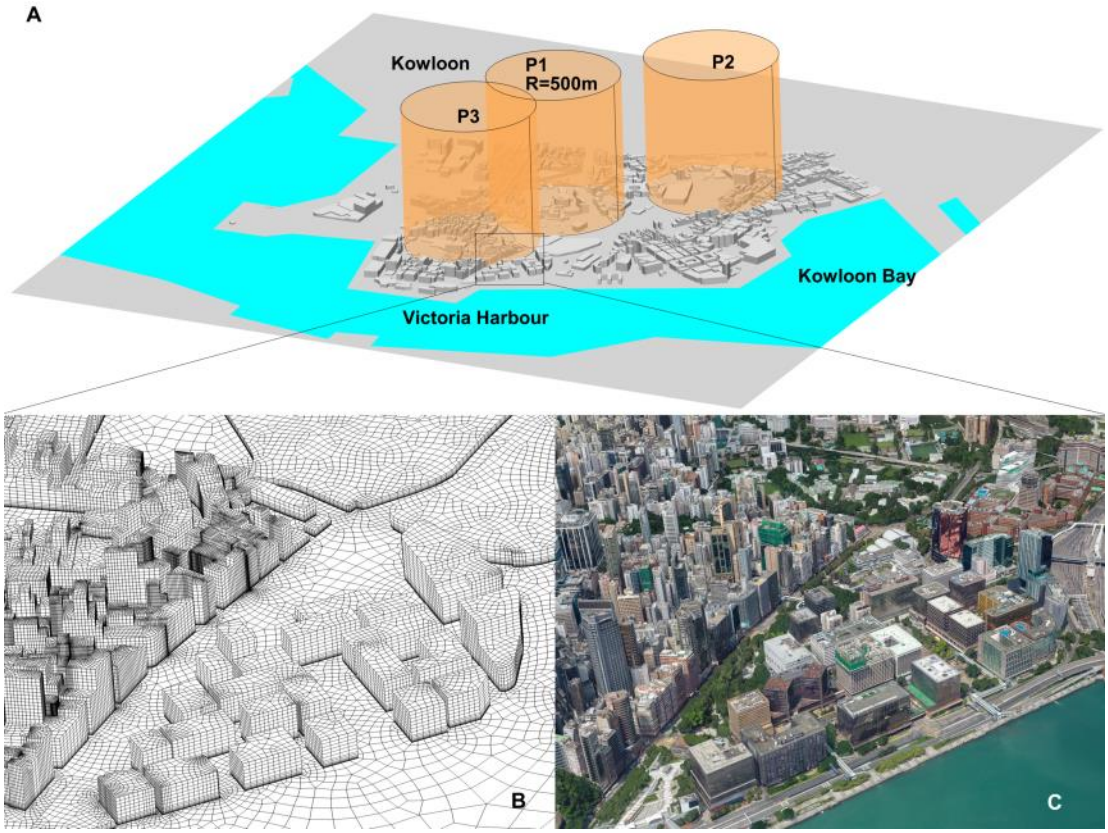

Fig. 3. (A) Locations of three averaged circular zones, P1, P2, and P3; (B, C) a part of the mesh of Case H and the corresponding latest (2018) perspective view extracted from Google Earth.

The realizable k-ε model was chosen, as it is generally accurate, reliable, computationally affordable, and widely used, following previous recommendations [21-23]. The AIJ has conducted extensive comparisons between CFD simulations and wind-tunnel measurements with a focus on steady RANS simulations [25]. Airflows around two types of single high-rise buildings, a high-rise building in a city, and two types of actual building complexes were compared comprehensively. Their results have shown that the k-ε model can predict the flow with fairly good accuracy, especially for relatively large wind speeds. Large eddy simulation (LES) can provide more accurate results and more details on the turbulence and other transient characteristics, but is also much more computationally costly. In our preliminary test, the realizable k-ε model with extruded mesh performed well on an AIJ benchmark case (Tominaga et al. [26], and more details can be found in the supplementary information). We therefore used the realizable k-ε model, considering the balance of computational costs and accuracy.

The pressure–velocity coupling scheme was the SIMPLE algorithm. The Green–Gauss node-based method was used for the gradient. Second-order discretization schemes were adopted

for the pressure equation. A second-order upwind scheme was used for both the convection and viscous terms. The convergence was determined from the residuals and the properties at several monitored points. The simulations were terminated when the monitored values did not change after at least 20000 iterations, and the residuals did not show any notable reduction.

Table 1. List of simulated cases

Case	Year	MAE (m)	Cell number (million)
A	1964	2.83	12.6
B	1975	2.18	13.2
C	1980	1.92	13.7
D	1985	2.52	13.9
E	1995	1.66	14.1
F	2000	3.25	14.5
G	2005	0.83	14.6
H	2010	0.81	14.9

Note: MAE denotes the mean absolute error of reconstructed building height

2.3 Boundary conditions

Kowloon Peninsula is mainly exposed to easterly wind, as shown later, and here we focus on studying the historical changes of the wind environment under easterly background wind. The wind speed of 3 m/s at a reference height of 10 m is taken as a threshold because it represents approximately 50% of the wind speed and is sufficiently strong that the buoyancy effect can be ignored.

The inlet velocity profile of easterly wind is given by a power law [23]:

$$u(z) = U_{ref} \times (\frac{z}{h_{ref}})^{\alpha}$$

where U_{ref} is the reference velocity at reference height h_{ref}. The exponent α can be taken as 0.11 $\pm$ 0.03 for the wind over the ocean under conditions of near-neutral atmospheric stability [27]. U_{ref}, h_{ref}, and α are equal to 3 m/s, 10 m, and 0.11 respectively in this case. The turbulent energy and dissipation rate can be determined by [28]:

$$k(z) = \frac{u^{*2}}{\sqrt{C_{\mu}}}$$

$$\varepsilon(z) = \frac{u^{*3}}{\kappa(z + z_0)}$$

where κ is the von Karman constant (= 0.4), $C_{\mu} = 0.09$, u^* is the atmospheric boundary layer friction velocity, and z_0 is the aerodynamic roughness length.

To overcome the inconsistency between the physical roughness of the wall function and aerodynamic roughness [29], the modified roughness height is specified. $k_{s,\ ABL}$ is calculated by:

$k_{s,\ ABL} = 9.793 \frac{z_0}{C_s}$.

In this case $k_{s,\ ABL} = 0.0039$ given that the roughness length of open sea $z_0 = 0.0002$ m [30]. Note that even though this roughness modification method is derived based on a logarithmic velocity profile and constant shear stress with height, and standard *k*-ε model, it can still provide a horizontally homogeneous wind profile in this case. Symmetry boundary conditions are specified at the lateral and top boundaries and the outflow is specified at the outlet.

3. Results and Analysis

3.1 Changes of annual mean wind speed and prevailing wind

Fig. 4A illustrates the annual mean wind speed profiles at the four weather stations of HKO. The overall average wind speeds at WGL, above an open sea area, remained approximately constant from 1968 to 2015, and those at KT also showed no clear trend of increase or decrease, as KT is also located over a relatively open area. However, a significant reduction of the mean speed was measured at KP, by -0.6 m/s per decade from 1968 to 1995 and -0.12 m/s per decade subsequently. Note that the anemometer of KP station was relocated (within the station) in 1996 when the wind speed decreased to about 2 m/s. The elevation of the anemometer at KP was also increased from 78m to 90m above mean sea level in 1996. The average wind speed increased slightly at SF by 0.13 m/s per decade. This is due to the corner effect: when the wind is blocked by Kowloon city, the wind at the corner of the city is increased.

The temporal evolution of the annual frequency of winds exceeding various thresholds (Fig. 4B-D) indicates particularly heavy suppression of wind speeds exceeding 3 m/s at KP. In contrast, the annual frequency of the various wind speeds neither increased nor decreased at SF. The annual frequency of wind speeds exceeding 9 m/s, which was always less than 10%, declined slightly at KT, but for the other thresholds the frequencies did not change significantly at that station. Correspondingly, Fig. 4E and 4F represent the historical plan area and building volume in the resolved region in this study. From 1964 to 2010, the plan area and building volume increased by 65% and 317% respectively in the investigated area.

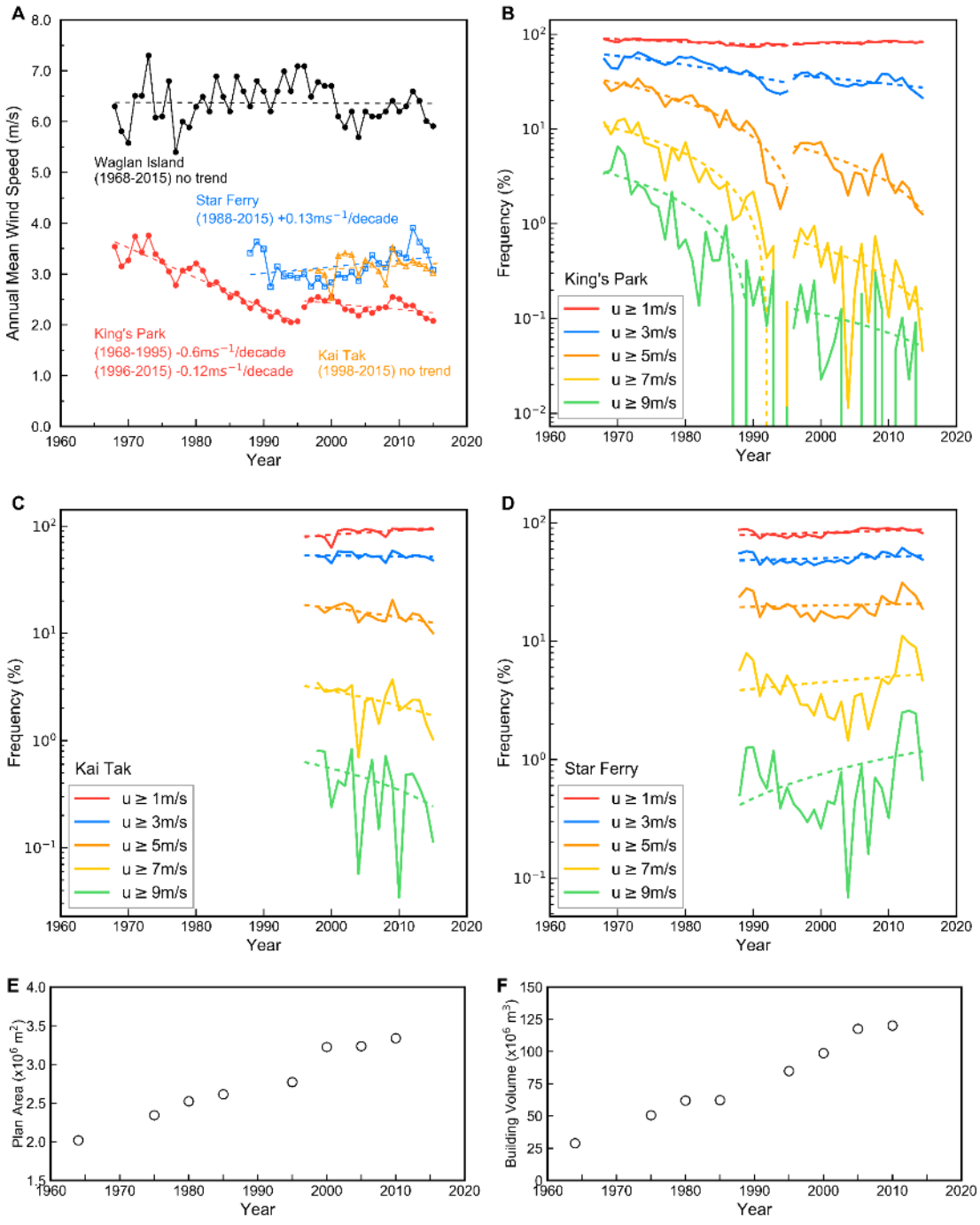

Fig. 4. Evolution of the annual wind speed and building volume. (A) evolution, as a function of year, of annual mean wind speed (based on 12-hourly observations ?) at four weather stations in Hong Kong (various colors); (B–D) evolution, as a function of year, of the annual frequency of wind speeds exceeding a given threshold (various curves, see legend) at King's Park (B), Kai Tak (C), and Star Ferry (D), the dash lines denote the linear regressions; (E) change of building plan area in the studied region from 1964 to 2010; (F) change of total building volume in the studied region from 1964 to 2010.

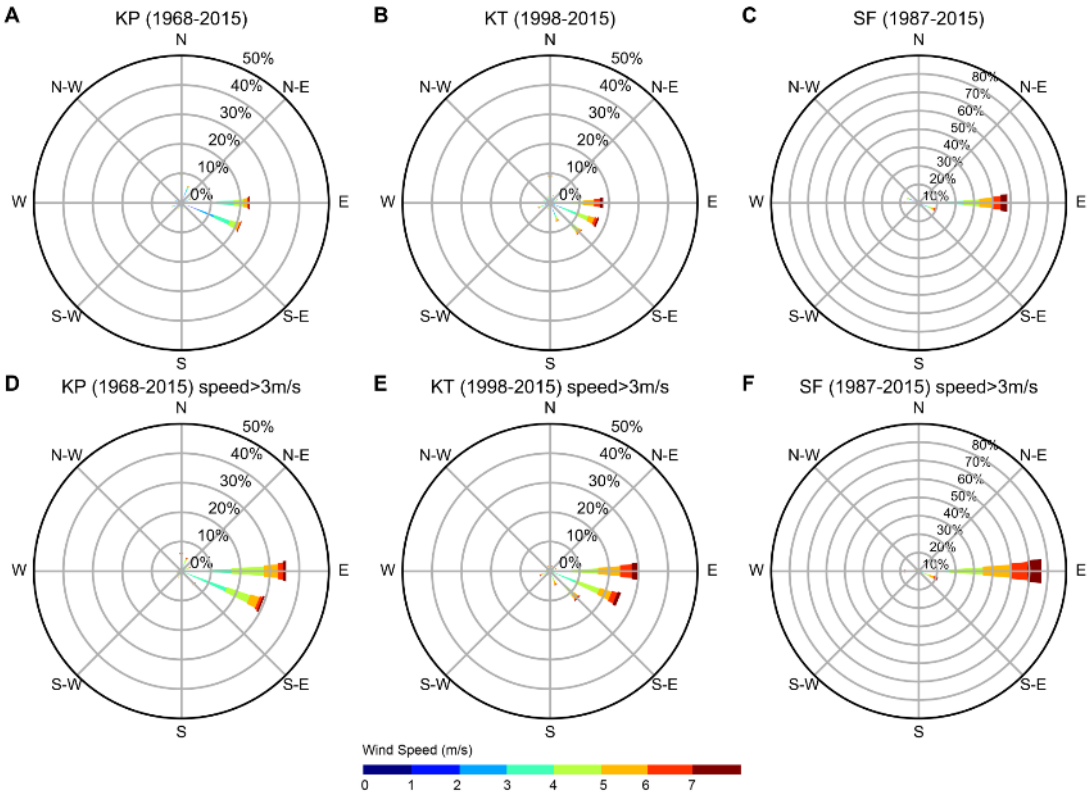

Fig. 5. Wind roses at three stations. (A) Wind rose at King's Park; (B) Wind rose at Kai Tak; (C) Wind rose at Star Ferry; (D) Wind rose at King's Park for wind speeds larger than 3 m/s; (E) Wind rose at Kai Tak for wind speeds larger than 3 m/s; (F) Wind rose at Star Ferry for wind speeds larger than 3 m/s.

The prevailing wind direction was easterly at KT and KP (Fig. 5), for the whole spectrum of wind speed. For the moderate winds or above, i.e. greater than 3 m/s, the prevailing wind was especially dominated by the easterly winds. The SF station, located at the southern tip of the Kowloon Peninsula bordering Victoria Harbour, is also mainly exposed to winds from the east. For winds stronger than 3 m/s, the frequency of easterly wind is about 70% at SF. Blockage of the prevailing easterly wind by new buildings is increasingly preventing wind from penetrating the city directly through built-up areas and streets. Consequently, greater amounts of wind are now diverted across Victoria Harbour. This is one possible reasons for the slight increase in average wind speed at SF, in particular during the later years.

3.2 CFD validation

The measured wind speeds at three stations, KP, SF, and KT, were used to validate the accuracy of the simulation. The elevations of the anemometers at KP, SF, and KT above mean sea level are 90 m, 18 m, and 16 m, respectively.

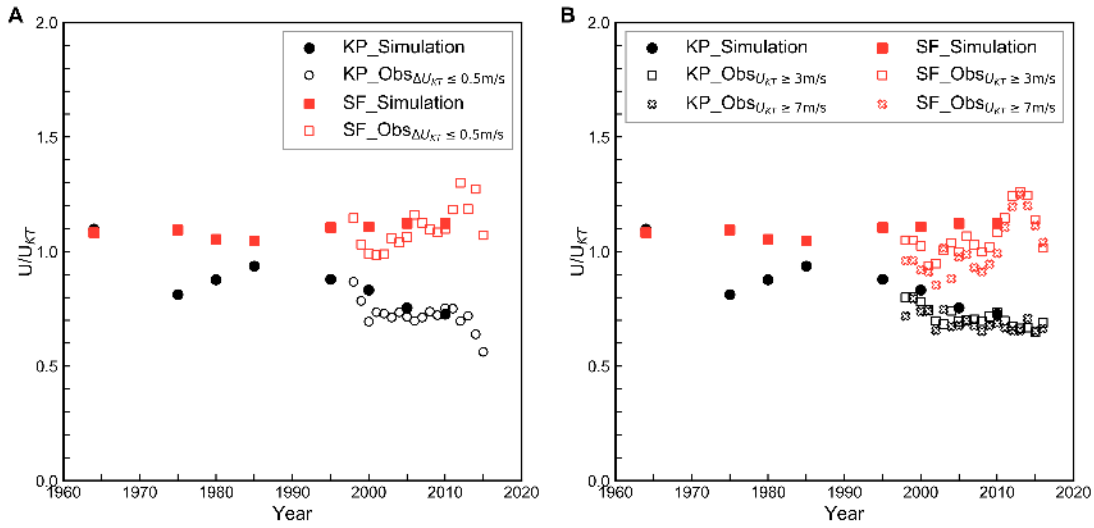

Fig. 6. Comparison of the dimensionless wind speed at King's Park (KP) and Star Ferry (SF) under two different conditions. A: for $\Delta U_{KT} \le 0.5\text{m/s}$; B: when the measured wind in Kai Tak (KT) exceeded a given threshold (various symbols, see legend).

Fig. 6 shows the simulated dimensionless wind speeds at KP and SF normalized by the wind speed at the same height of KT based on the inlet profile, and the observed dimensionless mean wind speeds calculated by:

$$\frac{U}{U_{KT}} = \frac{\overline{U_{KP(SF),syn}}}{\overline{U_{KT,E,Cond}}}$$

where *E* denotes that the hourly mean wind direction at KT is between 78.75 and 101.25 degrees (easterly wind). *Cond* denotes the conditions for selecting the measured wind speed at KT. Here we use two conditions: one is that the difference between observed and inlet velocity at KT, that is $\Delta U_{KT} = \left| U_{KT,Obs} - U_{KT,inlet} \right|$, is within 0.5 m/s, and the other is that the wind speed at KT is equal to or larger than a threshold wind speed. *syn* denotes synchronous wind speeds at KP or SF when at one of the two conditions mentioned above is satisfied. The frequency of the first condition is 19% for the easterly wind, while for the second condition, the frequency of easterly wind exceeding 3 m/s is 85%.

The conditional average is adopted because the instantaneous historical background wind varied over time, making it difficult to choose one specific year to validate the simulation results. Given a strong prevailing easterly wind, we can assume that the ratio of wind speeds is solely determined by the building layouts. Therefore, it is reasonable to compare the ratio of the conditionally averaged wind speed in each year, rather than comparing the absolute wind speed. Moreover, as 85% of the easterly wind at KT exceeded 3 m/s, it is acceptable to validate the simulation using only the data within this range.

As shown in Fig. 6, the simulated wind speed at KP gradually decreased from the 1960s to the present, while no notable change of wind speed occurred at SF. The simulated results agree well with the measurements. However, the measured wind speed at SF noticeably fluctuates compared with the simulation. The dimensionless wind speed calculated when the mean wind speed at KT exceeded a given threshold is plotted in Fig. 6B. For the two thresholds of 3 m/s and 7 m/s, the dimensionless velocities fluctuate in a similar manner

within narrow ranges. Note that with the increase of threshold speed, the dimensionless wind speeds in KP and SF both decreased slightly, i.e. the red and black crosses, which represent the larger wind speed threshold in Fig. 6B, are always at lower values than the other data points. This supports the argument that under windy conditions, the wind stilling phenomenon is more notable at urban sites (Fig. 4B).

3.3 Predicted overall wind change

The urban canopy layer consists of a fluid part (void with air) and a solid part (buildings). In summarizing the change of overall wind, it remains debated whether the averaging volume should exclude or include the solid part. The solid-exclusive average, known as the intrinsic spatial average (ISA), is widely used because of its clear physical meaning, while the solid-inclusive average, or comprehensive spatial average (CSA), is also important, especially for the one-dimensional parametrization of momentum flux, scalar transport, etc. [31]. In addition, the ISA of wind speed is quite useful for estimating the convective heat exchange coefficient of the external wall. The results of the two methods do not differ significantly, hence we only focus on the results for the ISA, while those for the CSA are shown in Supplementary Information.

Three circular areas, P1, P2, and P3, with radius R = 500 m, at the center of the computational domain, were chosen to investigate the general wind change (Fig. 3A). These locations were chosen for representativeness, as P1 covers KP station, P2 is in an upstream area, and P3 is in a high-rise and highly compact area.

The vertical distributions of the dimensionless horizontally mean wind speed, calculated by the ISA in these areas are presented in Fig. 7. The simulated velocity gradually decreased from 1964 to 2010. The reduction of relative wind speed (normalized by U_{ref}) was very significant at lower altitude. The wind speed below 50 m has become very small since 2000. Before 1990, the wind loss was very slight above 100 m. However, at P3, the wind speed has decreased considerably even above 100 m (Fig. 7C). Therefore, even high-rise buildings higher than 100 m have also been affected by wind loss.

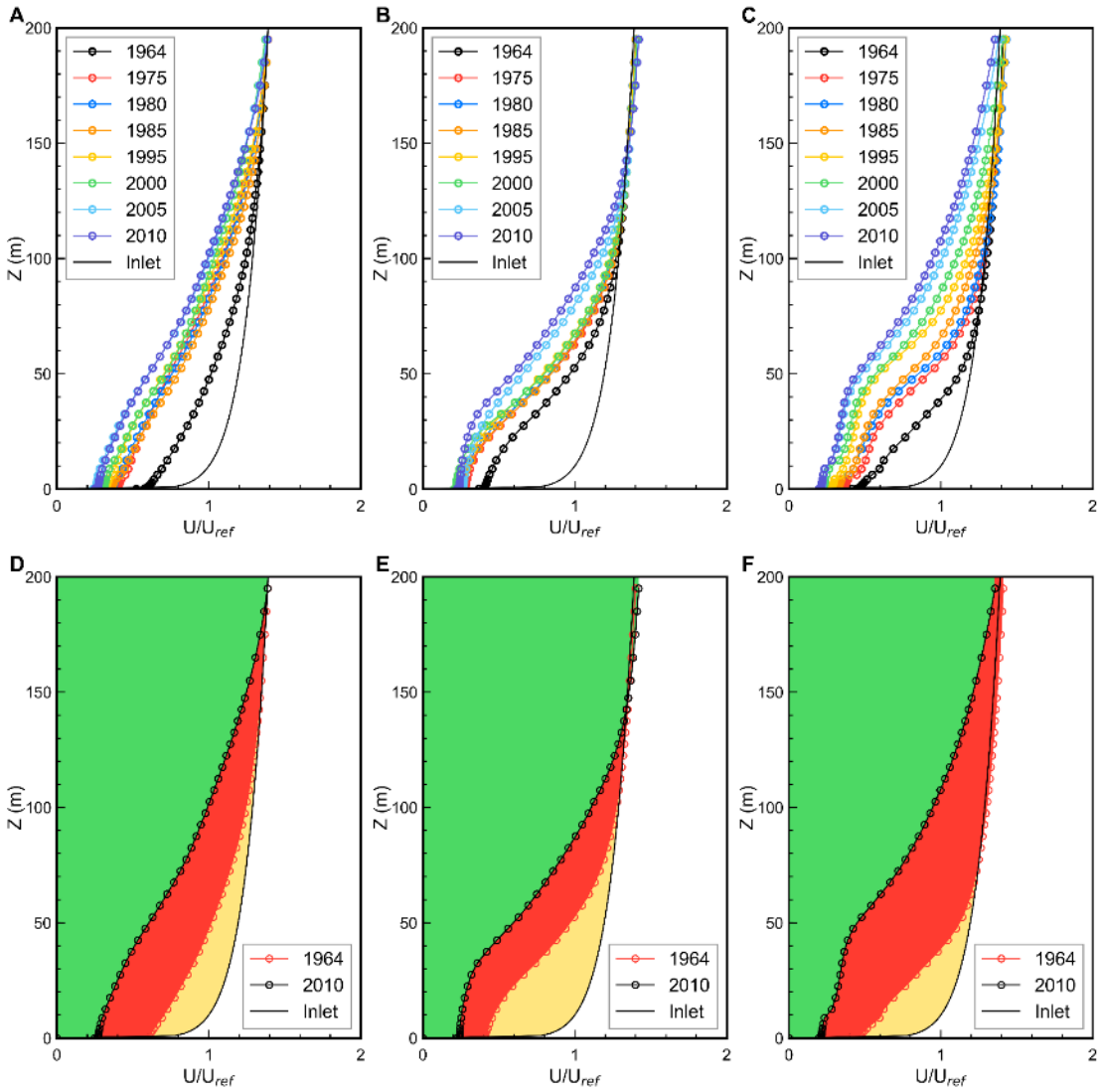

Fig. 7. Evolution of wind speed, wind loss, and wind resource calculated by intrinsic spatial average (ISA) in zones P1 (A, D), P2 (B, E), and P3 (C, F). Yellow, red, and green zones in D, E, and F denote the wind loss in 1964, additional wind loss in the period 1964-2010, and available wind resource in 2010, respectively.

Once the wind profile is obtained, the wind resource (WR) available between z_1 and z_2 can be computed by:

$$WR = \int_{z_1}^{z_2} u_{local}(z)dz$$

In Fig. 7D-F, the green areas represent the WR available in 2010, and the yellow areas represent the wind loss in 1964. The effect of urbanization from 1964 to 2010, i.e. the additional wind loss in this period, is represented by the red zones.

The local wind loss rate (WLR) between z_1 and z_2 can be computed by:

$$WLR = 1 - \frac{\int_{z_1}^{z_2} u_{local}(z)dz}{\int_{z_1}^{z_2} u_{inlet}(z)dz}$$

where $\frac{\int_{z_1}^{z_2} u_{local}(z)dz}{\int_{z_1}^{z_2} u_{inlet}(z)dz}$ is the sectional dimensionless wind resource. The total wind loss rate, as discussed later, can be calculated with z_1=0m and z_2=200m.

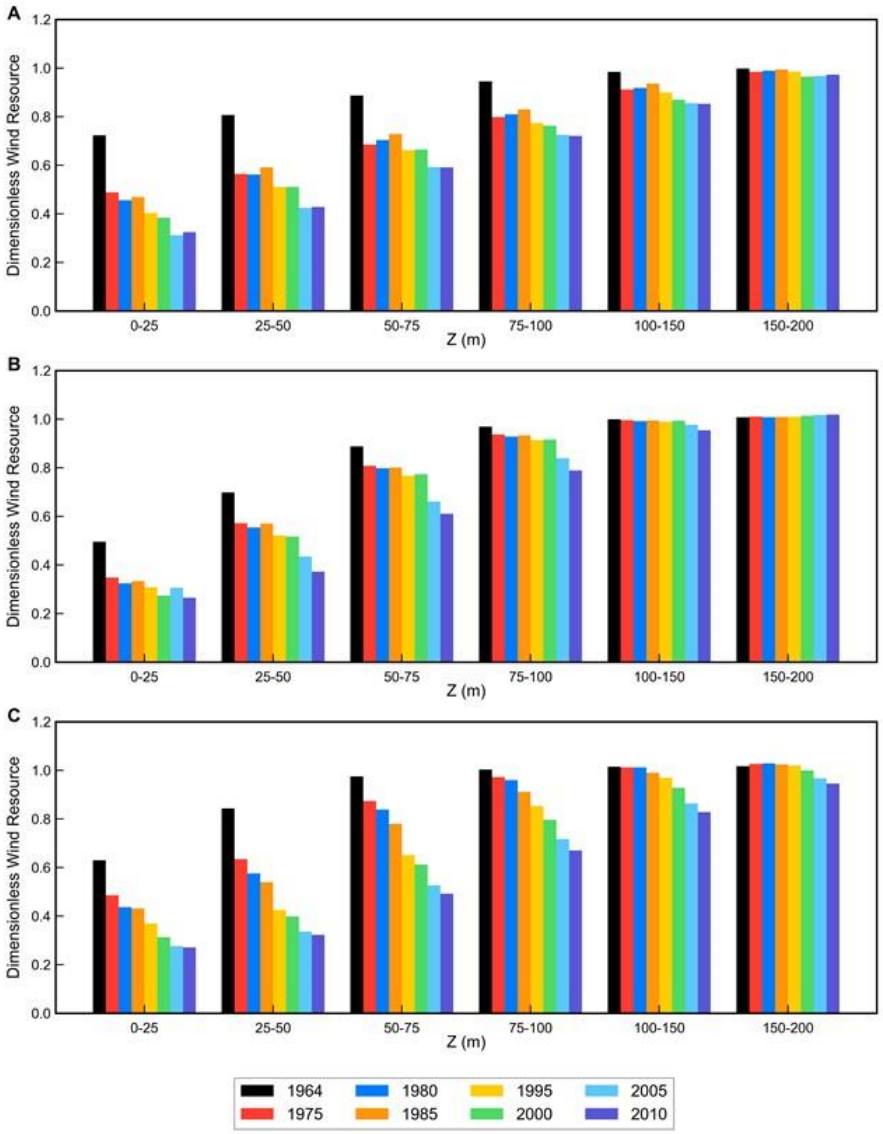

Fig. 8. Evolution of sectional dimensionless wind resource by intrinsic spatial average at different elevation intervals in zones P1 (A), P2 (B) and P3 (C).

To analyze the vertical distribution of the wind weakening, we also computed the sectional dimensionless wind resource at 6 elevation intervals, that are 0-25m, 25-50m, 50-75m, 75-100m, 100-150m and 150-200m, and the results are shown in Fig. 8. The most significant wind reduction occurred in the first 25m for all three zones P1, P2 and P3. Even in P1, the dimensionless wind resource had already declined from 72.3% to only 32.5% below z=25m (Fig. 8A). In P3, the wind reduced almost linearly below z=100m at different elevation intervals. For z =100m-150m and z =150-200m, the wind started to reduce in 1980 and 1995 respectively. This was attributed to the influence of new high-rise buildings and displacement. The wind loss rates at z=25-50m in P1, P2 and P3 had already increased to more than 50% in 2005. As shown in Fig. 8C, for z=50-75m in P3, the wind reduced from almost 97.5% to only 49.2%. The corresponding wind loss rate, that is about 10% per decade, is much more significant than other zones.

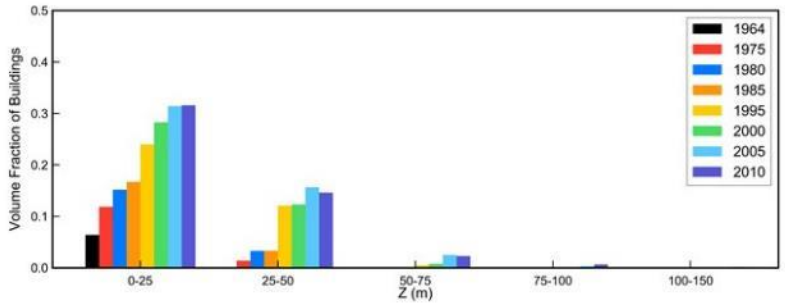

Fig. 9. Evolution of sectional volume fraction of buildings at different elevation intervals in the upstream of P3.

The vertical difference in wind weakening may be explained by the vertical difference in building volume change. As shown in Fig. 9, below elevation of 50m, there was a significant increase of volume fraction of buildings in the upstream of P3, with area of 2.1km×1km. Even though the volume fraction of buildings between 50-75m was very small, the wind reduction was remarkable. For lower level, the sectional wind reduction was caused by blockage of buildings. The wind profile was displaced, leading to a wind reduction in the upper level.

The total WLRs within z=200m calculated by the ISA and CSA in P1, P2, and P3 are shown in Fig. 10 as the wind reduction was notable in this region. Linear increases of WLR, with different slopes, are observed. Among the three studied regions, the wind reduction is most notable in P3, while that in P2 is the smallest. By linear regression, the total WLRs calculated by the ISA are 3.6%, 2.2%, and 5.8% per decade in P1, P2, and P3 respectively. In 1964, the wind reduction was less than 10% in each area. Remarkably, however, by 2010 even the smallest wind reduction was larger than 20%. The total WLR will exceed 40% by 2050 in both P1 and P2 if the current trend of wind loss continues.

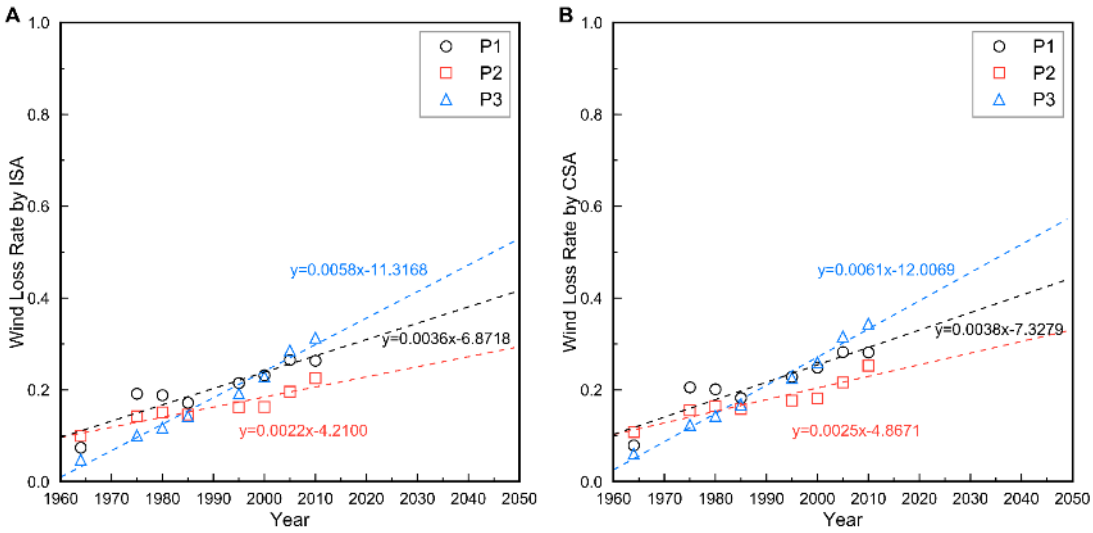

Fig. 10. Temporal change of the wind loss rate within z=200m calculated by (A) intrinsic spatial average (ISA) and (B) comprehensive spatial average (CSA) between 1964 and 2010, with extrapolation to 2050.

As shown in Table 2, the sectional volume fraction of buildings in the upstream of P3 and sectional WLR by ISA in P3 are significantly correlated within 100m, with vertically decreasing correlation coefficients. The change of wind in future might of course deviate from the linear increase as shown Fig. 10.

Table 2. Correlation coefficient of the sectional volume fraction of buildings in the upstream of P3 and sectional WLR by ISA in P3

z (m)	Correlation Coefficient
0-25	0.98
25-50	0.92
50-75	0.87
75-100	0.86

3.4 Pedestrian wind

As mentioned earlier, the reduction in wind speed below 50 m has become very significant since 2000. The pedestrian wind has a profound impact on the local thermal comfort and pedestrian safety. The distributions of dimensionless pedestrian wind speed, normalized by the inlet speed at z = 2 m, of Case A, C, F, and H are shown in Fig. 11. The wind speed mostly if not always became lower than the background wind speed, and by 2010 the wind at pedestrian level had become very small across almost the whole city (Fig. 11H). It is also noted that wind weakening not only occurs in building blocks, but also in leeward open spaces. Comparing Fig. 11A and 11H, we can see that the affected leeward area of the city had expanded significantly by 2010.

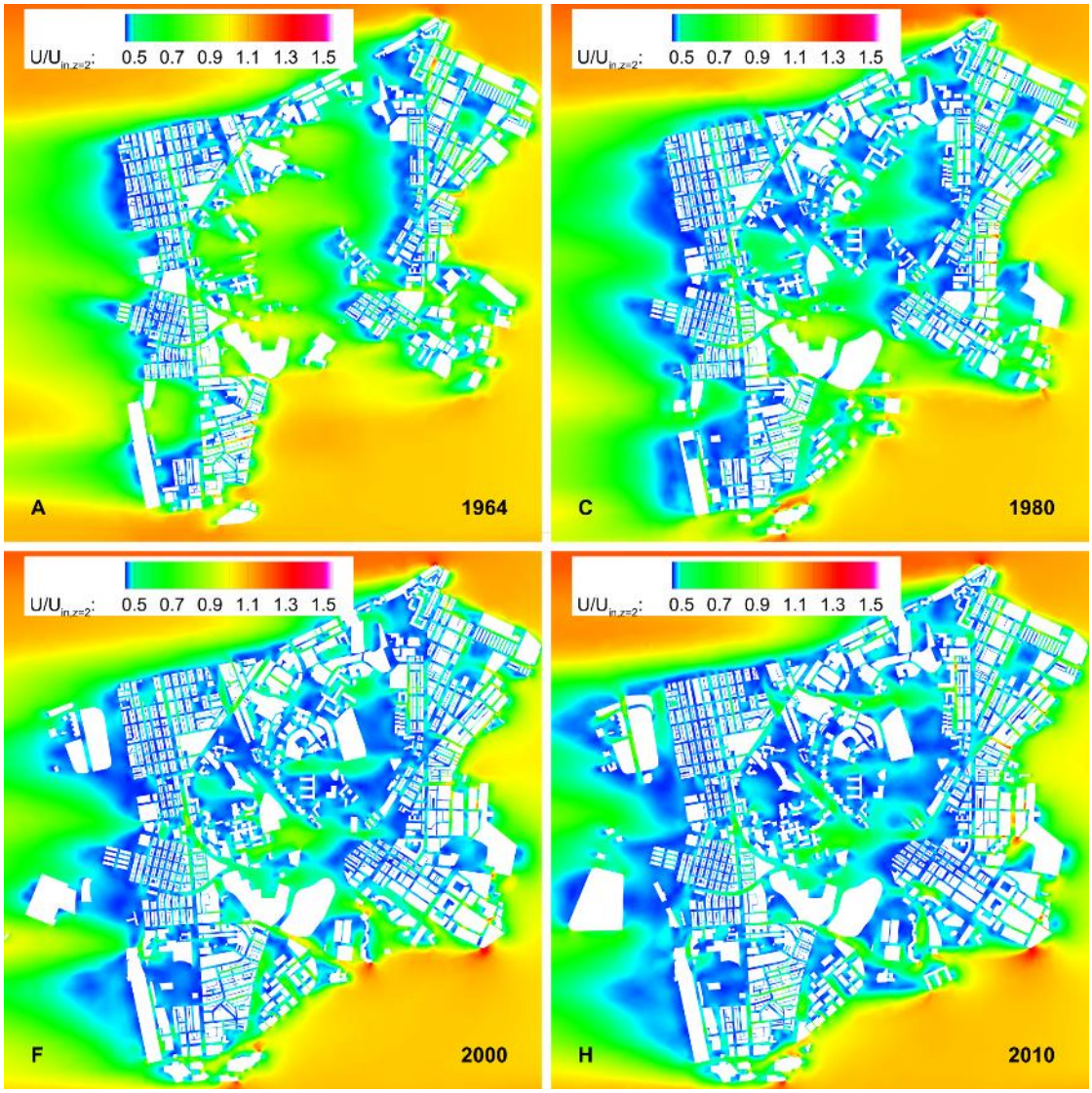

Fig. 11. Distributions of normalized pedestrian wind speed at Z = 2 m in A: 1964, C: 1980, F: 2000, and H: 2010

Despite the general wind reduction, in some areas the airflow was locally accelerated, as a result of the channel effect, Venturi effect, corner effect, and downwash vortex [32]. However, the regions of acceleration are much smaller than the areas of wind weakening, especially for those accelerations caused by the corner effect. The channeled accelerated flow can penetrate several building blocks, but the corner flow is not able to penetrate streets. In fact, the building density in Kowloon is too high to create large airflow channels. Therefore, the winds are mostly blocked, and the acceleration is negligible. Moreover, the wind speed at some open spaces in the downstream area or within the city is still rather low, because the volume/mass of air that can reach those areas is quite limited.

From the latest distribution of wind speed (in 2010, Fig. 11H), the existence of possible ventilation paths, where the wind speed is relatively large, may be identified. However, the building configuration is highly disordered and random, so the regions in which wind can be accelerated or at least maintained by these paths is very small. Peng et al. [33] attempted to identify the wind paths of least resistance in Kowloon based on the frontal area index (FAI). However, our CFD results indicate that the ventilation paths are only on the neighborhood-

scale but not the city-scale. This illustrates that while a coarse-grained approach can provide a certain level of information, CFD simulation can provide more details of the urban ventilation, especially the inhomogeneous distributions of wind acceleration or deceleration. It is recommended that a comprehensive CFD study be performed before the construction of new buildings in the future, considering the importance for the city of protecting and expanding these paths.

3.5 Impact of land reclamation

Land reclamation and associated urban development play a significant role in blocking of the wind. As shown in Fig. 1C, the Kowloon Peninsula has been significantly expanded since the 1960s [34] (an interactive land reclamation map can be found at http://www.oldhkphoto.com/coast/Map.html). In southeast Kowloon, many high-rise buildings have been built since 1964 on the reclaimed land. In the center of Kowloon, however, the buildings are older in age and lower in height. In addition, the protection of a large amount of land in the city center has transformed Kowloon into a bowl-shaped city, with higher buildings on the city perimeter and lower buildings in the middle. This distinctive urban morphology is an unintended consequence of two effects: the popular preference for buildings with views of the sea, and the high financial and labor costs of land reclamation. Consequently, high-rise buildings are an attractive choice for developers to achieve rapid recovery of construction costs.

As shown in Fig. 11F and 11H, even in open spaces in the center of the city, the pedestrian wind is quite weak. This reflects the blocking of approaching airflows by buildings immediately upstream. Therefore, the bowl-shaped morphology prevents winds from ventilating the Kowloon Peninsula , a common problem for coastal cities with densely built-up coastlines.

3.6 Limitations of this study

The influence of heat transfer and associated buoyancy-driven flows has not been analyzed. Buoyancy-driven flows should play an important role in influencing the city's climate, in particular when the background wind is weak. This is one way in which the buildings can directly influence the wind. Moreover, the building-affected wind could modify the heat transfer between ambient air and buildings, as well as the building energy consumption. We expect that urban blockage will not play a significant role when the background wind is weak; rather, the low winds will strengthen the buoyancy-driven flow effects, such as wall flows and urban heat island circulation [35, 36]. Other effects ignored in this study include those of surrounding mountains, transient characteristics, and atmospheric structure, such as stratification of the atmospheric boundary layer. These factors will be studied in the near future.

4. Conclusions

In this study, the historical change of wind environment in the Kowloon Peninsula, Hong Kong was investigated by CFD simulations. Simulations were performed in eight of the 47 years from 1964 to 2010 under prevailing easterly wind. In general, the predicted wind speeds agree well with the observed wind data at KP and SF meteorological stations. Vertical distributions of wind speed were calculated in three representative regions, namely P1, P2, and P3. The simulated results show that the overall mean wind speed decreased gradually in the studied period. New buildings provide significant blockages to the easterly wind. The

intensity of wind reduction was quantified by the WLR. In 1964, the wind reduction was less than 10% at all stations. Remarkably, by 2010, even the lowest recorded wind reduction was larger than 20%. By linear regression, the total WLRs were calculated in terms of the ISA as 3.6%, 2.2%, and 5.8% per decade in P1, P2, and P3, respectively. The total WLRs are projected to exceed 40% by 2050 in both P1 and P2 by extrapolating the current wind loss trends.

The airflow does undergo local accelerations in some parts of the Kowloon Peninsula, with the aid of specific building configurations, via the Venturi effect, channel flow, downwash vortex, and corner flow. However, according to our simulations, the accelerated wind is confined to limited areas, compared with the wind-stilling areas. Several decades of land reclamation and urbanization have transformed Kowloon into a bowl-shaped city in terms of building height. This results in the immediate blocking of wind by the upstream buildings as it approaches the urban center, which prevents the city from receiving adequate wind. Our study shows that continuing urbanization on the time scale of several decades can lead to significant wind stilling. The wind weakening phenomenon in urban areas of Hong Kong highlights the impact of dense urban development on the air ventilation. City planners and designers thus need to pay more attention to the long-term effects of development on the urban climate and environment.

Acknowledgements

This work is supported financially by an RGC CRF project (HKU9/CRF/12G) of the Hong Kong SAR Government, and a NSFC project (no 51278440).

References

[1] Guo, H., Xu, M., and Hu, Q. (2011). Changes in near-surface wind speed in China: 1969-2005. *International Journal of Climatology, 31*(3), 349-358.

[2] Mishra, V., Ganguly, A. R., Nijssen, B., and Lettenmaier, D. P. (2015). Changes in observed climate extremes in global urban areas. *Environmental Research Letters, 10*(2), 024005.

[3] Vautard, R., Cattiaux, J., Yiou, P., Thépaut, J.-N., and Ciais, P. (2010). Northern Hemisphere atmospheric stilling partly attributed to an increase in surface roughness. *Nature Geoscience, 3*(11), 756-761.

[4] Santamouris, M., Papanikolaou, N., Livada, I., Koronakis, I., Georgakis, C., Argiriou, A., et al. (2001). On the impact of urban climate on the energy consumption of buildings. *Solar Energy, 70*(3), 201-216.

[5] Lopes, A., Saraiva, J., and Alcoforado, M. J. (2011). Urban boundary layer wind speed reduction in summer due to urban growth and environmental consequences in Lisbon. *Environmental Modelling & Software, 26*(2), 241-243.

[6] United Nations. (2014). World Urbanization Prospects: The 2014 Revision, Highlights. Department of Economic and Social Affairs, Population Division, United Nations.

[7] Ginn, W. L., Lee, T. C., and Chan, K. Y. (2010). Past and future changes in the climate of Hong Kong. *Journal of Meteorological Research, 24*(2), 163-175.

[8] Hong Kong 2016: The Facts. (2016). *Hong Kong Yearbook 2016, Information Services Department of the Hong Kong SAR*.

[9] Ng, E. (2009). Policies and technical guidelines for urban planning of high-density cities: Air ventilation assessment (AVA) of Hong Kong. *Building and Environment, 44*(7), 1478-1488.

[10] Liu, J., Gao, Z., Wang, L., Li, Y., and Gao, C. Y. (2017). The impact of urbanization on wind speed and surface aerodynamic characteristics in Beijing during 1991–2011.

Meteorology and Atmospheric Physics,1-14.
[11] Hou, A., Ni, G., Yang, H., and Lei, Z. (2013). Numerical analysis on the contribution of urbanization to wind stilling: an example over the greater Beijing metropolitan area. *Journal of Applied Meteorology and Climatology, 52*(5), 1105-1115.
[12] Feddersen, B. (2005). Wind tunnel modelling of turbulence and dispersion above tall and highly dense urban roughness. Doctoral Thesis, Swiss Federal Institute of Technology, Zurich.
[13] Kastner-Klein, P., and Rotach, M. W. (2004). Mean flow and turbulence characteristics in an urban roughness sublayer. *Boundary-Layer Meteorology, 111*(1), 55-84.
[14] Klein, P., Leitl, B., and Schatzmann, M. (2007). Driving physical mechanisms of flow and dispersion in urban canopies. *International Journal of Climatology, 27*(14), 1887-1907.
[15] Hang, J., Sandberg, M., and Li, Y. (2009). Effect of urban morphology on wind condition in idealized city models. *Atmospheric Environment, 43*(4), 869-878.
[16] Ng, E., Yuan, C., Chen, L., Ren, C., and Fung, J. C. H. (2011). Improving the wind environment in high-density cities by understanding urban morphology and surface roughness: a study in Hong Kong. *Landscape and Urban Planning, 101*(1), 59-74.
[17] Xie, Z. T., and Castro, I. P. (2009). Large-eddy simulation for flow and dispersion in urban streets. *Atmospheric Environment, 43*(13), 2174-2185.
[18] Ashie, Y., and Kono, T. (2011). Urban-scale CFD analysis in support of a climate-sensitive design for the Tokyo Bay area. *International Journal of Climatology, 31*(2), 174-188.
[19] Tominaga, Y., Mochida, A., Shirasawa, T., Yoshie, R., Kataoka, H., Harimoto, K., et al. (2004). Cross comparisons of CFD results of wind environment at pedestrian level around a high-rise building and within a building complex. *Journal of Asian Architecture and Building Engineering, 3*(1), 63-70.
[20] Peng, F., Wong, M. S., Ho, H. C., Nichol, J., and Chan, P. W. (2017). Reconstruction of historical datasets for analyzing spatiotemporal influence of built environment on urban microclimates across a compact city. *Building and Environment, 123*, 649-660.
[21] Franke, J., Hirsch, C., Jensen, A. G., Krüs, H. W., Schatzmann, M., Westbury, P. S., Miles, S. D., Wisse, J. A., and Wright, N. G. (2004). Recommendations on the use of CFD in wind engineering. *Proceedings of the International Conference on Urban Wind Engineering and Building Aerodynamics*, in: van Beeck, J. P. A. J. (Ed.), COST Action C14, Impact of Wind and Storm on City Life Built Environment, von Karman Institute, Sint-Genesius-Rode, Belgium, May 5-7, 2004.
[22] Blocken, B., van der Hout, A., Dekker, J., and Weiler, O. (2015). CFD simulation of wind flow over natural complex terrain: case study with validation by field measurements for Ria de Ferrol, Galicia, Spain. *Journal of Wind Engineering and Industrial Aerodynamics*, *147*, 43-57.
[23] Tominaga, Y., Mochida, A., Yoshie, R., Kataoka, H., Nozu, T., Yoshikawa, M., et al. (2008). AIJ guidelines for practical applications of CFD to pedestrian wind environment around buildings. *Journal of Wind Engineering and Industrial Aerodynamics, 96*(10-11), 1749-1761.
[24] van Hooff, T., and Blocken, B. (2010). Coupled urban wind flow and indoor natural ventilation modelling on a high-resolution grid: a case study for the Amsterdam ArenA stadium. *Environmental Modelling & Software, 25*(1), 51-65.
[25] Yoshie, R., Mochida, A., Tominaga, Y., Kataoka, H., Harimoto, K., Nozu, T., et al. (2007). Cooperative project for CFD prediction of pedestrian wind environment in the Architectural Institute of Japan. *Journal of Wind Engineering and Industrial Aerodynamics, 95*(9-11), 1551-1578.
[26] Tominaga, Y., Yoshie, R., Mochida, A., Kataoka, H., Harimoto, K., and Nozu, T. (2005).

Cross comparisons of CFD prediction for wind environment at pedestrian level around buildings: comparison of results for flowfield around building complex in actual urban area. *The Sixth Asia-Pacific Conference on Wind Engineering* (APCWE-VI), Seoul, Korea, September 12-14, 2005.
[27] Hsu, S. A., Meindl, E. A., and Gilhousen, D. B. (1994). Determining the power-law wind-profile exponent under near-neutral stability conditions at sea. *Journal of Applied Meteorology, 33*(6), 757-765.
[28] Richards, P., and Hoxey, R. (1993). Appropriate boundary conditions for computational wind engineering models using the k-ϵ turbulence model. *Journal of Wind Engineering and Industrial Aerodynamics, 46*, 145-153.
[29] Blocken, B., Stathopoulos, T., and Carmeliet, J. (2007). CFD simulation of the atmospheric boundary layer: wall function problems. *Atmospheric Environment, 41*(2), 238-252.
[30] Wieringa, J. (1992). Updating the Davenport roughness classification. *Journal of Wind Engineering and Industrial Aerodynamics, 41*(1-3), 357-368.
[31] Xie, Z. T., and Fuka, V. (2017). A note on spatial averaging and shear stresses within urban canopies. *Boundary-Layer Meteorology,* 1-9.
[32] Gandemer, J. (1975). Wind environment around buildings: aerodynamic concepts. *In Proc., 4th Int. Conf. Wind Effects on Buildings and Structures*, Heathrow, 1975, 423-432.
[33] Peng, F., Wong, M. S., Wan, Y., and Nichol, J. E. (2017). Modeling of urban wind ventilation using high resolution airborne LiDAR data. *Computers, Environment and Urban Systems, 64*, 81-90.
[34] Survey & Mapping Office (1996). Reclamation & Development in Hong Kong. *Lands Department of Hong Kong*, Series AR/9/RD, Edition 4
[35] Fan, Y., Li, Y., Hang, J., Wang, K., and Yang, X. (2016). Natural convection flows along a 16-storey high-rise building. *Building and Environment*, *107*, 215-225.
[36] Fan, Y., Hunt, J. C. R., and Li, Y. (2017). Buoyancy and turbulence-driven atmospheric circulation over urban areas. *Journal of Environmental Sciences*, *59*, 63-71.

Supplementary Information

S.1 Validation on a benchmark case

Due to the lack of historical measurements in Kowloon, a validation based on observations at three meteorological stations is not sufficient. It is important to analyze the numerical settings and grid arrangements to ensure that the simulations are accurate.

The geometries studied here are highly complex, as there are thousands of buildings in each case and the length scale ranges from 10^{-2} m to 10^{3} m. This creates difficulties in generating a high-quality mesh. With a tetrahedral mesh, which is relatively easy to generate, the total cell number needed for good performance could be hundreds or even thousands of millions. The corresponding computational costs would be beyond the means of most researchers and engineers, including our team. Using a structured mesh can reduce the cell number, but it is impossible to manually deal with 10^{3} to 10^{4} wall surfaces. Therefore, the mesh generation technique presented by van Hooff and Blocken [24] was adopted. The mesh was generated by sweep and extrusion of a 2D surface mesh, and only hexahedral and prismatic cells were created.

Before simulating the wind environments in Kowloon, a preliminary simulation with the same mesh generation method and numerical settings was conducted on a well-known Architectural Institute of Japan (AIJ) benchmark case, described in Ref. [26]. The AIJ study involved a wind-tunnel experiment on an urban complex in Niigata, Japan, at a scale of 1:250 (relative to the actual complex size of 500m × 500m × 300m), and obtained pedestrian-level wind speeds at 80 locations. Fig. S1A shows the building configuration and Fig. S1B shows the mesh configuration. The total cell number is only 2.36 million. Note that the domain does not extend far in the horizontal directions, as suggested by AIJ guidelines, but instead follows the geometry in Tominaga et al. [26]'s study. Airflow driven by westerly background wind was simulated. The profiles of inlet velocity, turbulence kinetic energy, and dissipation rate were interpolated using experimental data. The lateral and top boundaries were specified as symmetry and the outlet boundary was specified as a zero pressure outlet.

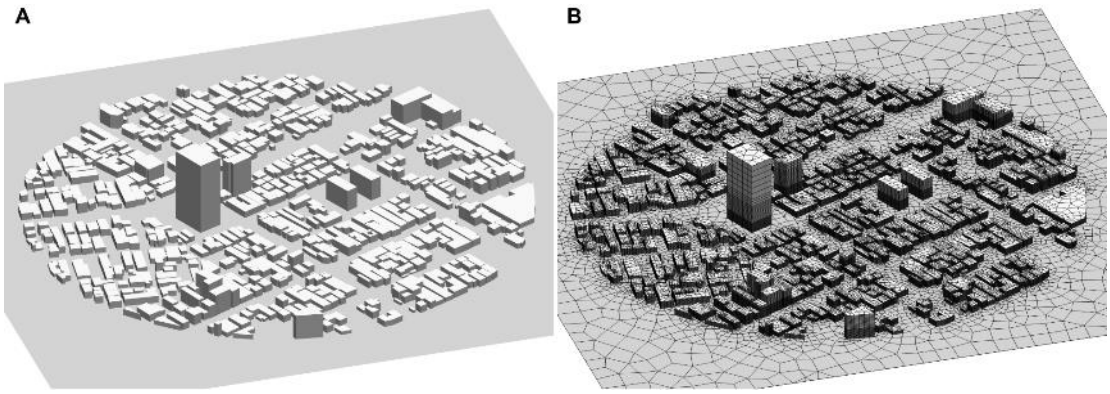

Fig. S1. (A) Building configuration and (B) mesh of the benchmark case.

Fig. S2 compares the numerically simulated vs. experimental values of the normalized scalar velocity, which is defined as the ratio of the wind speed at each measurement point (height = 2 m) to the wind speed at the same height at the inflow boundary. The simulation–experiment comparison is made for the present study (Fig. S2A) and for Tominaga et al. [26] (Fig. S2B). The predicted velocities generally agree well with the experiments for most data points.

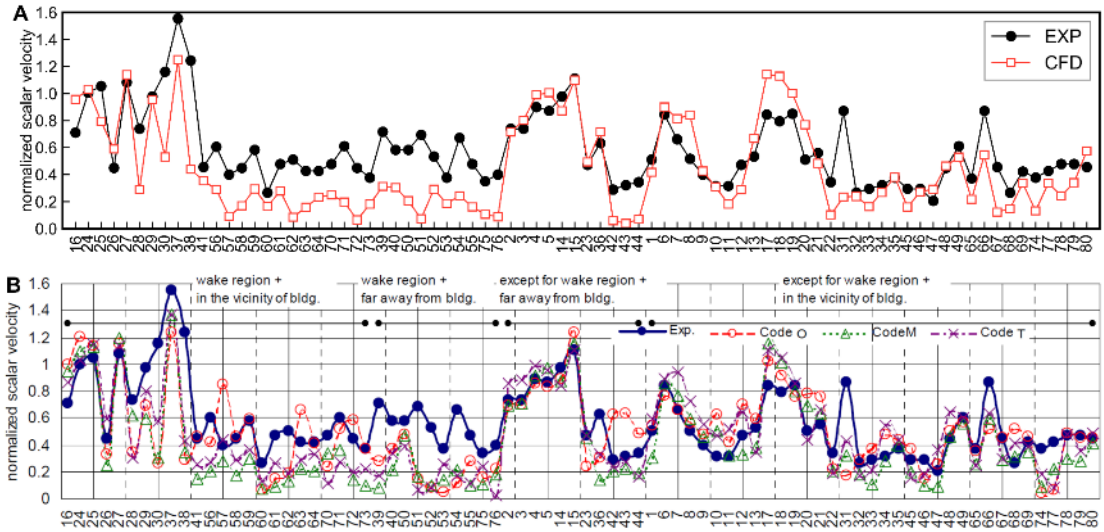

Fig. S2. Comparison of the simulated normalized scalar velocity and the corresponding values from wind-tunnel experiment. (A) Comparison between present simulation and experiment. EXP and CFD denote experimental and simulated data, respectively. (B) Comparison between simulation and experiment from Tominaga et al. [26].

S.2 Analysis of grid sensitivity and domain size

Having found that the realizable k-ε model with surface extruded mesh performed well on the benchmark case, we concluded that it was suitable for simulating the airflows in Kowloon. Three meshes for Case H (year 2010) were compared to analyze the grid sensitivity. The total cell numbers of the coarse, medium, and fine meshes were 6.3 million, 14.9 million and 22.3 million, respectively. The vertical distributions of mean velocity in P1, P2, and P3 are compared in Fig. S3. The difference is negligible even between the results of the coarse mesh and fine mesh. Thus, the medium mesh can be assumed to yield grid-independent results. In addition, the coarse mesh can be used to calculate the averaged wind speed if the local details of airflow are not of interest.

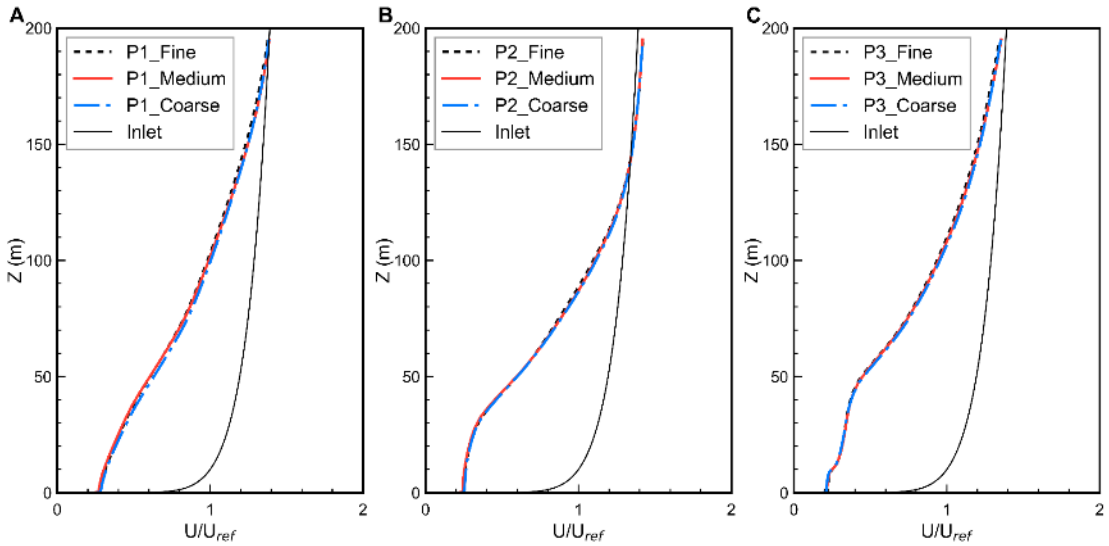

Fig. S3. Vertical distributions of normalized mean wind speed predicted by coarse, medium, and fine meshes at P1 (A), P2 (B), and P3 (C).

In addition to sufficient grid resolution, appropriate extensions in the horizontal and vertical directions are necessary for simulations of the airflow around buildings. The AIJ recommends that the inlet, lateral, top, and outflow boundaries should be placed 5H, 5H, 5H, and 10H away from the buildings to avoid unexpected acceleration in the lateral direction, and obtain fully developed flow in the downstream [23]. For urban areas, COST (European Cooperation in the Field of Scientific and Technical Research) recommends that lateral boundaries be extended by 2.3W (where W is the width of the built area) and outflow boundaries by 15H [21]. However, Tominaga et al. [23] argued that COST's recommendation may be conservative. Whether the AIJ's recommendation is suitable for this study is not clear. Therefore, a comparison of Case H (2010) between standard and large domains was conducted to analyze the influence of domain size. The standard domain was defined based on the AIJ's recommendation, while the large domain was more conservative, with additional extensions of 3 km in the lateral directions and 7 km in the downstream. The normalized mean wind speeds in P1, P2, and P3 for Case H (2010) are presented in Fig. S4. The difference between domain sizes is negligible at each location. As the built areas of the other cases are smaller than in Case H, the AIJ's recommendation on the domain extensions can be considered sufficient for this study.

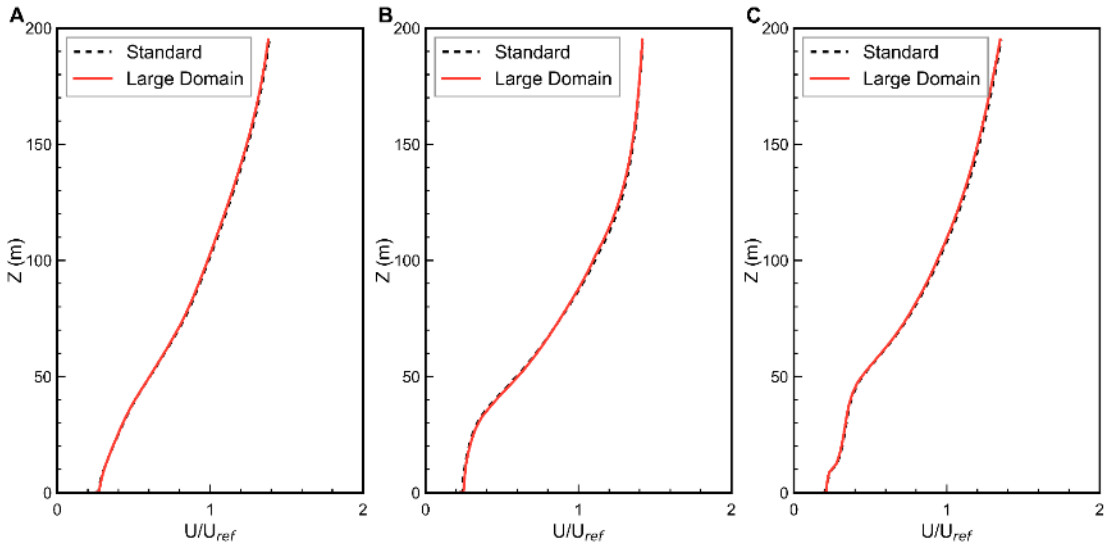

Fig. S4. Vertical distribution of normalized mean wind speed predicted with standard domain and large domain at P1 (A), P2, (B) and P3 (C).

Based on the benchmark validation and analysis of the grid sensitivity and domain size sensitivity, we can conclude that the realizable k-ε model and surface extrusion technique are suitable to investigate the wind environment of complex urban settings. The AIJ's recommendations on the distances of the inlet, lateral, top, and outflow boundaries are sufficient, while the COST's recommendations are too conservative for this study.

S.3 Comprehensive spatial average

Because the comprehensive spatial average includes buildings, the resulting mean wind speeds are always smaller than those of the intrinsic spatial average. The difference between wind loss rates calculated by ISA and CSA is not significant (Fig. 8) at elevations within 200 m. However, as shown in Fig. S5, the streamwise wind speed at lower levels can become very small, especially at the pedestrian level. For P2 and P3, the streamwise wind speed below 10 m is never greater than 10% of the reference wind speed. However, the ISA wind speed can reach as high as around $0.2U_{ref}$ (i.e. 20%). The results of these two methods indicate that the ventilation can be reduced near the ground level.

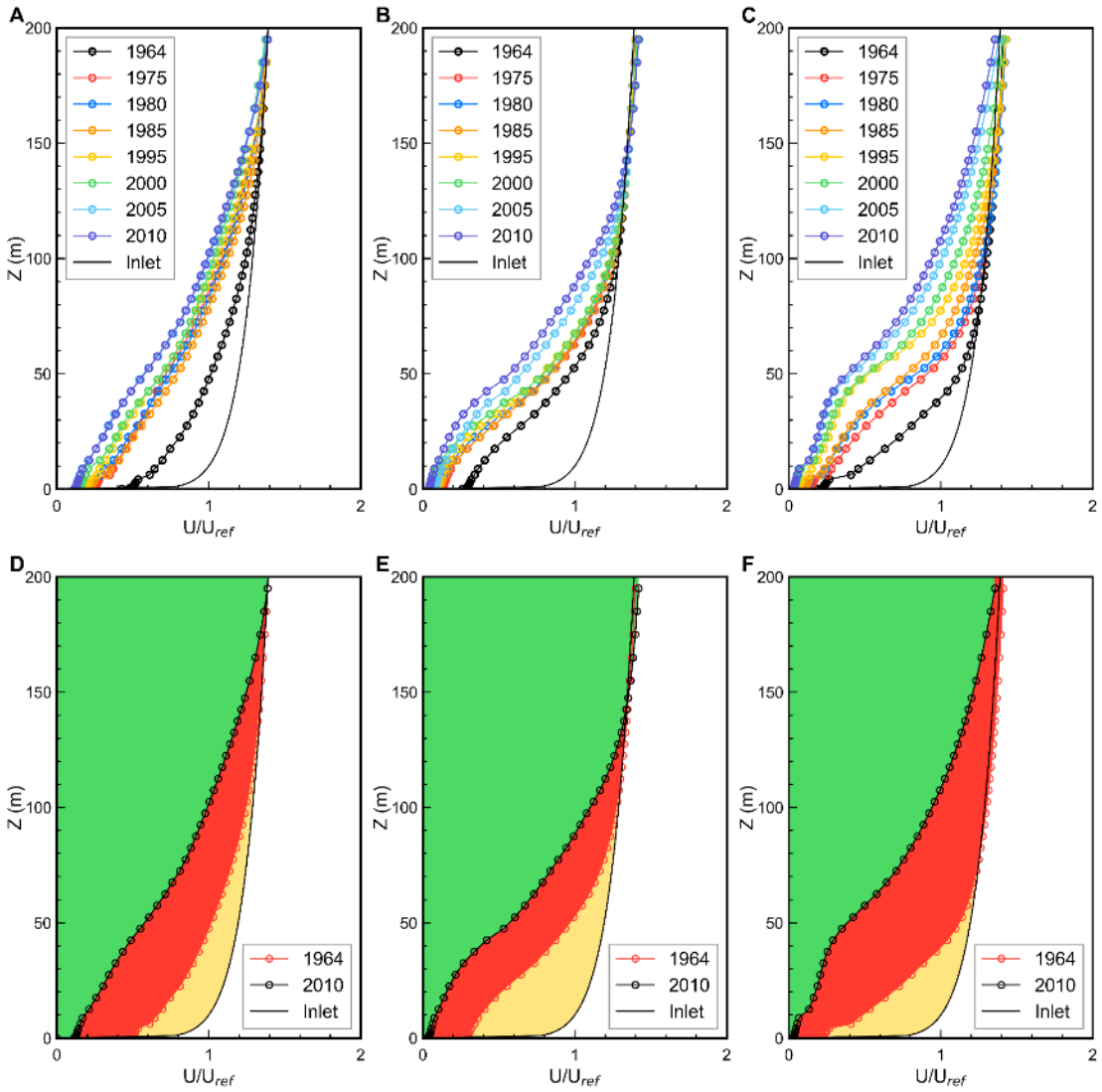

Fig. S5. Evolution of wind speed, wind loss, and wind resource calculated by comprehensive spatial average (CSA) in P1 (A, D), P2 (B, E), and P3 (C, F). Yellow, red, and green zones in D, E, and F denote the wind loss in 1964, additional wind loss in the period 1964-2010, and available wind resource in 2010, respectively.